Optimising tidal range power plant operation

Athanasios Angeloudis*, Stephan C. Kramer, Alexandros Avdis, Matthew D. Piggott

Department of Earth Science & Engineering, Imperial College London, UK

HIGHLIGHTS

- We describe numerical methods to simulate the operation of tidal range power plants.
- We couple simplified power plant operation models with gradient-based optimisation algorithms.
- The consideration of a flexible operation with pumping is shown to have the potential to deliver significant energy gains.
- Optimisation of larger plant designs should be coupled with hydrodynamics solvers.

ARTICLE INFO

ABSTRACT

Tidal range power plants represent an attractive approach for the large-scale generation of electricity from the marine environment. Even though the tides and by extension the available energy resource are predictable, they are also variable in time. This variability poses a challenge regarding the optimal transient control of power plants. We consider simulation methods which include the main modes of operation of tidal power plants, along with algorithms to regulate the timing of these. This paper proposes a framework where simplified power plant operation models are coupled with gradient-based optimisation techniques to determine the optimal control strategy over multiple tidal cycles. The optimisation results inform coastal ocean simulations that include tidal power plants to gauge whether the benefits of an adaptive operation are preserved once their hydrodynamic impacts are also taken into consideration. The combined operation of two prospective tidal lagoon projects within the Bristol Channel and the Severn Estuary is used as an example to demonstrate the potential benefits of an energy maximisation optimisation approach. For the case studies considered, the inclusion of pumping and an adaptive operation is shown to deliver an overall increase in energy output of 20–40% compared to a conventional two-way uniform operation. The findings also demonstrate that smaller schemes stand to gain more from operational optimisation compared to designs of a larger scale.

1. Introduction

Tidal range power plants harness the potential energy contained within coastal flows characterised by a high tidal range. Existing and prospective tidal range projects essentially constitute impoundments either in the form of *barrages* that span an entire estuarine basin [1,2], or as *coastal lagoons* positioned against coastlines [3]. These impoundments are designed to facilitate a potential head difference through the carefully orchestrated operation of sluice gates and hydro-turbines, with the latter converting potential energy into electricity. This technology has been gaining momentum, as indicated by a recent UK Government review [4] suggesting that it could make sustainable contributions to the nation's electricity needs in the near future, if developed strategically.

The design and operation of a tidal power plant needs to consider the minimisation of potential environmental impacts [5,2], the maximisation of power output [6] and meeting the electricity demand in a cost-effective manner among other factors. Given the significant capital investment required for the construction of tidal range plants [7] and the nascent status of the technology relative to other electricity generation methods, the optimal operating characteristics must be determined at the design stage enabling an informed quantification of investment risk and return.

The optimisation of tidal range structure operation in response to the time-varying resource represents an important challenge. Numerical simulations are typically used to examine the effect of various parameters on electricity output. However, the problem of determining the optimal operating parameters can be computationally demanding, as simulations must accurately resolve the plant near-field as well as the far-field conditions if the hydrodynamic response of the

---

flow is to be accurately predicted across all the scales relevant to the problem and for all parameter permutations.

Previous studies of tidal range power, including Prandle [8], Wolf et al. [5], Burrows et al. [9], Xia et al. [10,11], Falconer et al. [12], Cornett et al. [13], generally focused on: (a) conventional ebb-only/flood-only generation or two-way operation without pumping options; and (b) assumed that the operation remained uniform over varying tidal conditions. Very little has been reported in terms of optimisation; the study of Aggidis and Benzon [6] considered that the optimum head difference might vary subject to the tidal range present in an ebb-only strategy, which effectively corresponds to a single-variable optimisation problem. More recently, the optimisation of a simplified two-way operation in tidal power plants was presented by Lisboa et al. [14] heeding lessons from hydro-power scheduling optimisation studies [15]. Only a few control parameters and technical constraints have typically been considered, thus making exhaustive brute-force optimisation methods computationally feasible. Here we seek to build on preceding efforts through the application of an optimisation approach allowing for a far more flexible control of tidal power plant operation.

Current tidal lagoon proposals would likely feature dynamic operation strategies (e.g. bidirectional generation with pumping intervals [16]) that should be accounted for in their assessment. A realistic operation scenario involves a large number of variables, and optimisation using exhaustive variable-space investigations can progressively become computationally untenable. Gradient-based methods are increasingly popular for optimising parameters in complex engineering problems, without a wide exploration of the complete parameter space [17–19]. We present a gradient-based optimisation approach for the adaptive operation of tidal power plants, that is in addition informed by and tested using coastal ocean modelling simulations to account for the effects of the schemes on surrounding hydrodynamics.

2. Methodology

2.1. Tidal power plant operation

The potential energy contained within a head difference H developed across a tidal range structure, neglecting any form of losses, has been investigated by Prandle [8] and quantified as

$$E_{\max} = \frac{1}{2}\rho g A H^2,\qquad(1)$$

in J where ρ is the fluid density (kg/m^3), g is the gravitational acceleration (m/s^2), A is the impounded surface area (m^2), and

$$H = \eta_{\mathrm{up}} - \eta_{\mathrm{dn}},\qquad(2)$$

is the head difference developed where η_{up} and η_{dn} correspond to the upstream (i.e. on the inland side of the impounded area) and downstream (outer) water elevation respectively in m. The total amount of energy resource that can be extracted from a tidal power plant in each tidal cycle is related to (a) turbine technology capabilities, (b) the spring-neap (and longer period) tidal variations at the site and (c) the design of the structure and its interaction with local hydrodynamics.

The efficiency of tidal power plants in harnessing the available potential energy during a given tidal cycle is heavily dependent on the control of the constituent hydraulic structures [10,20,9,8,21]. A generalised illustration of how a plant can be regulated is presented in Fig. 1, with $t_i, i = 1,...,n$ forming the main control variables. In its simplest form, power generation is one-directional, i.e. it is restricted to either the ebb or flood stages of the tide. For example, in a typical ebb-only (without pumping) generation strategy the active modes of operation according to Table 1 are reduced to a sequence of $m = 2, 4, 6$ and 7a. In that case the only variable to be determined (following Fig. 1) is t_6, i.e. the holding time at $m = 6$ prior to power generation ($m = 7a$). The transitions to $m = 2$, $m = 4$ and $m = 6$ are triggered automatically once the minimum turbine generation head ($h_{\min}$) is

reached, for $H < 0$ and $H > 0$ respectively. In order to simulate the operation of such sequences in time, it is essential to parametrise the behaviour of turbines and sluice gates.

2.2. Hydraulic structure parametrisation

The flow through the power plant hydraulic structures is driven by the water head difference H developed between the two sides of the structure. H can be used as input to functions that calculate the instantaneous flow rate from turbines and sluice gates. Sluice gate flow Q_s (kg/m^3) can be calculated as:

$$Q_s(m,H,t) = \begin{cases} r(t)\cdot\mathrm{sgn}(H)\cdot C_d\cdot A_s\cdot\sqrt{2g|H|} & \text{for } m \in \{3b,4,7b,8\} \\ 0 & \text{otherwise} \end{cases}\qquad(3)$$

where A_s is the aggregate cross-sectional flow area (in m^2) of the gates installed, and $sgn(\cdot)$ returns the sign (-1 or 1) of a given quantity; in this case the head difference H. C_d is the sluice gate discharge coefficient that is dependent on the design of the sluice gates [21]. Higher C_d values imply that a lower sluice gate area (A_s) might be required and thus reduce construction costs; previous studies experimentally demonstrated that values higher than unity can be achieved [22,23] through sluice gate design modifications. For regional and far-field scale coastal ocean models a sensitivity test to the parameter C_d can be found in Bray et al. [24]. Nonetheless, a value of unity is normally selected within regional scale models [9,13] and this practice has been adopted here. A sinusoidal ramp function taking the values $r(t) = \sin(\pi/2 \times (t-t_m)/t_r)$ for $t \in [t_m, t_m + t_r]$, and unity otherwise, represents the transition at the beginning of a mode where t_r is the interval expected when opening hydraulic structures and t_m the time when the current mode was triggered. Similar expressions are imposed when closing the hydraulic structures.

The flow through turbine caissons is not reliably calculated using Eq. (3) as discussed previously [9]. Instead, hill chart parametrisations are preferable while power is generated to reflect the installed turbine characteristics [25]. If followed sequentially, the equations in Table 2 can be used to calculate the flow rate and the energy generated from a bulb turbine for a given H value. This yields the tidal turbine flow rate Q_t (m^3/s):

$$Q_t(m,H,t) = \begin{cases} -r(t)\cdot\mathrm{sgn}(H)\cdot N\cdot Q_p & \text{for } m \in \{1,5\} \\ r(t)\cdot\mathrm{sgn}(H)\cdot N\cdot Q_h(H) & \text{for } m \in \{3a,3b,7a,7b\} \\ r(t)\cdot\mathrm{sgn}(H)\cdot N\cdot C_t\cdot\sqrt{2g|H|}\cdot\pi D^2/4 & \text{for } m \in \{4,8\} \\ 0 & \text{otherwise} \end{cases}$$
$$(4)$$

where N is the number of turbines installed, Q_p (m^3/s) the pumping flow rate, Q_h (m^3/s) the flow rate according to the hill chart parametrisation of Table 2 and D (m) the turbine diameter. C_t is a nondimensional turbine discharge coefficient that is applied to the orifice equation. It scales the flow rate based on the transition between turbine generation and sluicing according to the turbine specifications. The power P_t (MW) produced from tidal range turbines can be expressed as:

$$P_t(m,H,t) = \begin{cases} -r(t)\cdot\rho\cdot g\cdot Q_p\cdot|H|/\eta_p & \text{for } m \in \{1,5\} \\ r(t)\cdot P_h(|H|) & \text{for } m \in \{3a,3b,7a,7b\} \\ 0 & \text{otherwise} \end{cases}\qquad(5)$$

where P_h (MW) is the power calculated from the sequence in Table 2 and η_p is a pumping efficiency which is a function of H [26].

2.3. Operation modelling

The simulation of the tidal power plant performance can be accomplished in several ways [9,27,28]. Essentially, the domain is split into downstream (outer) and upstream (inland) sub-domains connected at the hydraulic structure location. The downstream water levels
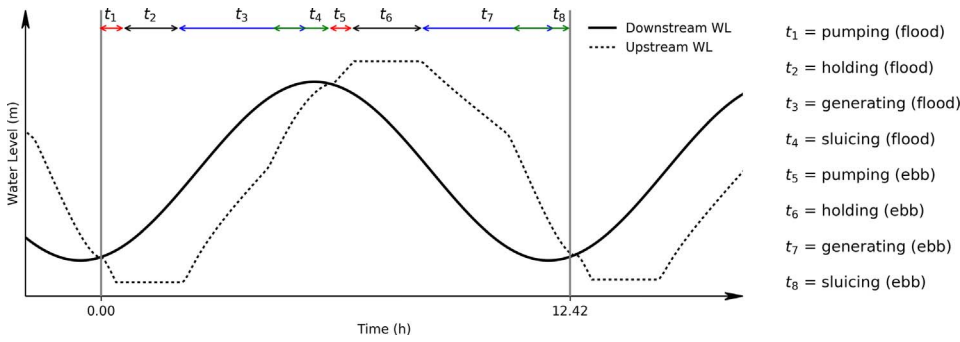
Fig. 1. Generalised operation of a tidal power plant over an M_2 tidal period, illustrating typical modes of operation. Red arrows represent consumption of energy, blue arrows generation periods and green the transfer of water volume from sluice gates. (For interpretation of the references to colour in this figure legend, the reader is referred to the web version of this article.)

t_1 = pumping (flood)

t_2 = holding (flood)

t_3 = generating (flood)

t_4 = sluicing (flood)

t_5 = pumping (ebb)

t_6 = holding (ebb)

t_7 = generating (ebb)

t_8 = sluicing (ebb)

Table 1

Control sequence and reference guide for the modes of operation m in a tidal power plant.

m	Operation Mode Description
1	Pumping water at flood tide (emptying)
2	Holding water at Low Water (preserving)
3a	Flood generation (filling)
3b	Flood generation with sluicing (filling)
4	Sluicing (filling)
5	Pumping water at ebb tide (filling)
6	Holding water at High Water (preserving)
7a	Ebb generating (emptying)
7b	Ebb generating with sluicing (emptying)
8	Sluicing (emptying)

Table 2

Parametrisation of a double-regulated bulb turbine applied in the tidal range energy resource assessments to calculate Power P_h and Discharge Q_h.

#	Formulations	Description
1	$S_p = \dfrac{2 \cdot 60 \cdot f_g}{G_p}$	Turbine speed S_p (rpm), where f_g is the grid frequency (Hz) and G_p the generator pole number
2	$n_{11} = \dfrac{S_p \cdot D}{\sqrt{|H|}}$	Unit speed n_{11} (rpm) where D is the diameter (m)
3	$Q_{11} = \begin{cases} 0.017 n_{11} + 0.49, & n_{11} \leqslant 255 \\ 4.75, & n_{11} > 255 \end{cases}$	Unit discharge Q_{11} from empirical equations of [6]
4	$Q^* = Q_{11} D^2 \sqrt{|H|}$	Discharge estimate Q^* (m^3/s) through turbine for H (m)
5	$P^* = \mathbf{min}(\rho g Q^* |H|, C_p)$	Power for Q^* subject to the turbine capacity C_p (MW)
6	$Q_h = \dfrac{P^*}{\rho g |H|}$	Correction of Q_* to determine Q_h in case of maximum capacity C_p
7	$\eta_h = -0.0019 n_{11} + 1.2461$	Empirical expression for hydraulic efficiency η_h [25]
8	$\eta_o = \eta_1 \cdot \eta_2 \cdots \eta_{n-1} \cdot \eta_n$	Consideration of other efficiency factors, e.g. turbine orientation, friction
9	$P_h = \rho g Q_h |H| \eta_o$	Power P_h (MW) calculated subject to efficiency losses

prescribed (0-D modelling) or predicted (in 1-D, 2-D and 3-D hydrodynamic modelling) are used to calculate H and thus the flows and power in time as described in Section 2.2.

2.3.1. Zero-dimensional modelling

Our 0-D model implementation is based on a backward finite difference method which adheres to the principles of mass conservation. A water level time-series $\eta_{dn}(t)$ that represents the downstream elevation locally to the site is used to calculate H and in turn determines the water volume exchanged at the current timestep enabling the calculation of an updated η_{up}:

$$\frac{d\eta_{up}}{dt} = \frac{Q_s(m,H,t) + Q_t(m,H,t) + Q_{in}}{A_s(\eta_{up})}, \tag{6}$$

where $A_s(\eta_{up})$ is a site-specific function for the wetted surface area of the tidal range structure (in m^2) assuming a constant water level of η_{up} across the entire upstream surface area. Q_{in} (in m^3/s) corresponds to the sum of inflows/outflows through independent sources such as rivers or outfalls.

2.3.2. Two-dimensional modelling

The drawback of 0-D models in neglecting the impact of tidal power plants on local and regional hydrodynamics can be significant for larger tidal lagoons and barrages [5,29]. To address this, regional coastal ocean models can be used to predict the flow elevations, velocities and the altered tide constituents. In this case, we use *Thetis*, a (2-D and 3-D) flow solver for simulating coastal and estuarine flows implemented using the *Firedrake* finite element Partial Differential Equation (PDE) solver framework [30]. *Thetis* was configured to solve the non-conservative form of the nonlinear shallow water equations:

$$\frac{\partial \eta}{\partial t} + \nabla \cdot (H_d \mathbf{u}) = 0, \tag{7}$$

$$\frac{\partial \mathbf{u}}{\partial t} + \mathbf{u} \cdot \nabla \mathbf{u} - \nu \nabla^2 \mathbf{u} + f \mathbf{u}^\perp + g \nabla \eta = -\frac{\tau_b}{\rho H_d}, \tag{8}$$

where η is the free surface perturbation, H_d is the total water depth and $\mathbf{u}$ is the depth-averaged velocity vector with horizontal components u, v while ν is the kinematic viscosity of the fluid. The term $f\mathbf{u}^\perp$ accounts for the Coriolis effect and comprises of $\mathbf{u}^\perp$, the velocity vector rotated counter-clockwise over 90° and $f = 2\Omega \sin(\zeta)$, with Ω the angular frequency of the Earth's rotation and ζ the latitude. Bed shear stress (τ_b) effects are represented through the Manning's n formulation expressed as:

$$\frac{\tau_b}{\rho} = g n^2 \frac{||\mathbf{u}|| \mathbf{u}}{H_d^{\frac{1}{3}}}. \tag{9}$$

Since intertidal areas can influence the tidal power plant performance, wetting and drying processes are treated according to the formulation of Kärnä et al. [31]. The model is implemented using a discontinuous Galerkin finite element discretisation (DG-FEM), using the $P_{1DG} - P_{1DG}$ velocity-pressure finite element pair. A semi-implicit Crank-Nicolson timestepping approach is applied for temporal discretisation with a constant timestep of Δt. The discretised equations are solved using a Newton nonlinear solver algorithm using the PETSc library [32]. In terms of boundary forcings, beyond the imposed water levels at the seaward boundaries and the river discharge fluxes along the coast, the representation of the turbines and sluice gates is implemented according to a flux-based method using the principles of domain decomposition [20]. Flux values are determined at each time step as described in Section 2.2 based upon sampling the water elevations adjacent to the turbines and sluice gates.

2.4. Operation optimisation

Tidal range structures differ from other sources of marine energy

(e.g. wave energy converters and tidal stream arrays) since to a certain extent they have flexibility over when they generate power. This means that the duration of the individual modes m (Fig. 1), e.g. the periods during which electricity is generated, can be optimised subject to the operational objectives and the transient tides. While various objectives could be considered, we investigate here the specific problem of maximising the electricity generated by the tidal lagoons. If we encode the duration of the modes in a vector, τ, where $\tau = \{t_i, i = 1,...,N\}$ the following objective function can be formulated:

$$E(\tau) = \int_{t=0}^{t=t_s} P(\tau,H,t)dt, \tag{10}$$

where t_s is the simulation time. $P(\tau,H,t)$ represents the transient power levels obtained from 0-D simulations. The combination of τ and t sequentially determines m that is necessary for Eqs. (3)–(5).

As the plant operation is cyclic (with a period of $T \approx 12.42$ h), the vector τ can be optimised independently for each tidal cycle, allowing the operation control points to adapt as transient tidal (e.g. spring-neap) conditions evolve. If the simulation spans $n_c = t_s/T$ cycles, with $n_c \in \mathbb{N}$ then we formulate the following problem:

for $i = 1 : n_c$

$$\max_{\tau_i} \quad \int_{t=i\times T}^{t=(i+1)\times T} P(\tau_i,H,t)dt$$

subject to $\quad \tau_l \leqslant \tau_i \leqslant \tau_u$ $\tag{11}$

where τ_l, τ_u correspond to the lower and upper limits expected for the different modes of operation, with a lower limit of zero allowing the operation to skip to the next mode of operation. The model input in each cycle depends on information from the previous tidal cycles' operation such as starting upstream water level, mode m and its duration. The gradient-based optimisation algorithm used to determine τ is the limited memory Broyden-Fletcher-Goldfarb-Shanno with bounds (L-BFGS-B) algorithm, an iterative method for solving nonlinear optimisation problems. This is packaged as part of SciPy and outlined in Zhu et al. [33]. For the purposes of this work the L-BFGS-B algorithm treats the 0-D model as a black box and approximates the gradient of the objective function with respect to τ by individually varying the vector's components. Optimising all the parameters simultaneously during prolonged periods would require the application of the 0-D model as many times as the number of parameters that need to be determined. There is therefore an incentive to decompose the optimisation problem in tidal cycle steps considering the algorithm's computational efficiency when calculating the gradient of fewer parameters, and iteratively running computationally lighter simulations.

2.5. Tidal energy case studies and hydrodynamic simulations

The Bristol Channel and the Severn Estuary region in the South West of the UK is considered as a case study for the determination of an efficient adaptive operation for potential power plants (Fig. 2). Due to the significant tidal range developed within the estuary, there is strong industrial interest in constructing tidal range structures in the area. We consider two tidal lagoon proposals, namely Tidal Lagoon Power Ltd's Swansea Bay and the Cardiff tidal lagoons proposed to cover 11.6 and ≈ 65 km^2 respectively. This complements previous hydrodynamic modelling studies that accounted for the simultaneous operation of tidal lagoons [27], but did not consider the advantages of adapting the operation control in time. As a starting point, we assume the turbine specifications of Table 3 and the lagoon shapes of Fig. 2(c–d).

The overall configuration and details of the designs (Fig. 2) are based on available information from existing tidal lagoon proposals [34–36] which include the size of the turbines and the technology selected. The shape of the lagoons has to balance geotechnical, environmental and economic constraints, all of which are beyond the immediate remit of this study [35,29]. Nonetheless, the location of the turbines and sluice gates requires sufficient water depth to ensure that certain components are consistently submerged to operate efficiently. For this reason they have been positioned in the deeper areas of the impoundment as shown in Fig. 2. In both designs, further dredging activities and bathymetry levelling may be required during construction to ensure the smooth installation of the turbines.

The mesh generation approach described by Avdis et al. [37,38] was followed to produce the multi-scale unstructured triangular meshes to discretise the study domain. Two meshes with the same resolution characteristics have been generated in order to consider the tidal hydrodynamics with and without the tidal lagoons present. The meshes are refined in the vicinity of the tidal lagoon structures as illustrated in Fig. 2(c–d) with the element sizes ranging from 2500 m at the outer boundaries to 20 m closer to the turbine and sluice gate locations. The baseline case comprised 27,754 nodes and 55,593 elements, whereas the one with the lagoons featured 35,021 node and 70,138 elements. The higher resolution of the latter is due to the mesh refinement around the turbines and sluice gate sections. In turn, the bathymetry was interpolated across the mesh with data from the Edina Digimap Service [39] at one arc-second resolution (≈ 30 m). The simulation results presented in this paper utilise a constant time-step Δt of 50s, which was decided upon following a sensitivity test.

The models were tidally forced using eight constituents ($M_2, S_2, N_2, K_1, Q_1, O_1, P_1, K_2$) available from the TPXO database [40] at the seaward boundaries and average river flows stemming from UK's National River Flow Archive data for inland open boundaries. Simulations, initially subjected to five days of spin-up time with respect to energy production and hydrodynamics, then spanned three full lunar months between 6 May 2003 and 6 Aug 2003. The starting simulation date was arbitrarily selected and is reported here for completeness. The main constraint for the simulations has been that their duration should be long enough to resolve the main tide constituents at sites of interest, e.g. immediately downstream of the tidal range structures, but also to span a sufficient amount of time to observe the benefits of an optimised plant control within the hydrodynamic model.

3. Results

3.1. Tidal range energy resource and hydrodynamics validation

Optimal design specifications of prospective tidal power plants will be dictated by the water elevation signal at proposed hydraulic structure sites. In order to obtain these for the Swansea Bay and Cardiff Lagoon configurations and also to assess the performance of the hydrodynamic models, an initial run was set up to simulate the established ambient (i.e. with no lagoons present) tide conditions within the Bristol Channel and the Severn Estuary. *Thetis*'s ability to accurately model the ambient tidal heights was assessed through comparisons with observational data that include tide gauge water level time series and tide constituents at five sites from the UK's National Tide Gauge Network (Fig. 3) recorded from earlier observational campaigns (Table 4). *Thetis*'s capability to capture the tidal range variation within the computational domain can be observed by the neap to spring tide transition of Fig. 3. The predicted tide constituents (Table 4) are similarly in good agreement with the available recorded data for the main semidiurnal constituents that dictate the local tidal conditions. Root Mean Squared Error (RMSE) values of 0.07, 0.04, 0.03 m and 2.80°, 2.02°, 2.14° were recorded for M_2, S_2, N_2 amplitudes and phases respectively. The model could be improved by refining/calibrating the setup with additional information, but this was considered beyond the immediate remit of this work given that the focus is on the relative tidal lagoon performance between simulations; for example, the Manning's n was set to a constant value of 0.023 s/m$^{1/3}$ across the entire domain for simplicity and this can contribute to localised deviations on the grounds of the sea bed morphology variation.

Water elevation time series close to the hydraulic structures can be used as an indicator for the potential tidal range energy available over
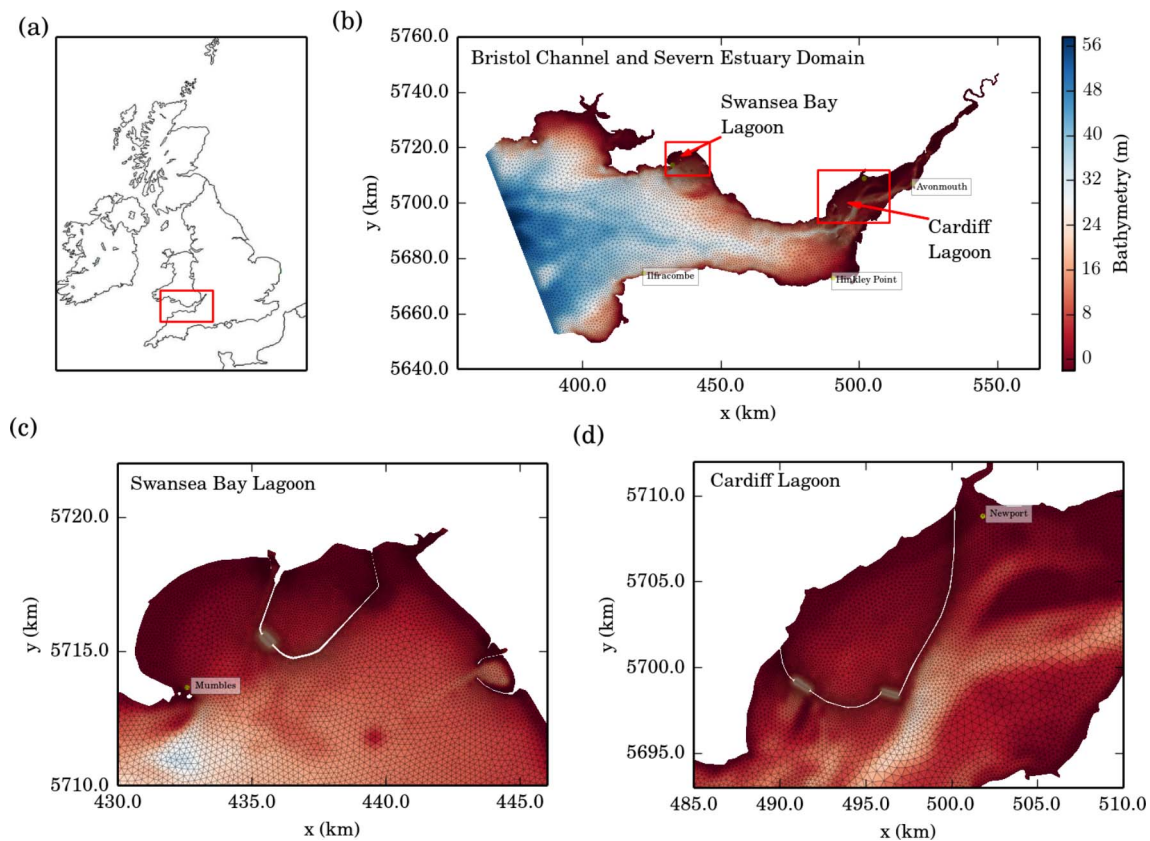
Fig. 2. (a) Study area relative to UK map, (b) Computational domain considered for the simulations in the Bristol Channel and the Severn Estuary, (c) Swansea and (d) Cardiff Lagoon configuration and unstructured mesh refinement.

Table 3
Tidal range bulb turbine specifications.

Specifications	Swansea Bay Tidal Lagoon	Cardiff Tidal Lagoon
Turbine D (m)	7.35	8.90
Generator poles G_p	95	113
Electricity grid frequency f_g (Hz)	50	50
Fluid density ρ (kg/m^3)	1025	1025
Turbine discharge coefficient (C_t)	1.36	1.36

time. Fig. 4(a) plots the reconstructed signal from the tide constituents (Table 5) obtained from the 2-D model over an extended period of time at the two sites. Using a peak detection algorithm, the water level difference for the transitions between high water (HW) and low water (LW) were isolated and are plotted as discrete values in time in Fig. 4(b). The tidal range values were then fed into Eq. (1) to yield an estimate of the potential energy contained in each transition from HW to LW and vice versa (Fig. 4(b)). Accumulating the potential energy over an entire year suggests that ≈ 92 and 156 GW h/km^2 are theoretically available at the Swansea and the Cardiff sites respectively; this demonstrates how the tidal resonance that amplifies the tidal range within the estuary (by an average of 30% from 6.62 m at Swansea to 8.63 m at Cardiff according to predictions stemming from the baseline hydrodynamic simulation of the domain) corresponds to $\approx 70\%$ more energy for every impounded km^2 as per Eq. (1).

3.2. Operation optimisation

The first objective of the optimisation considered is to define the number of turbines and uniform optimal operational characteristics (i.e.

a single optimised τ which is uniform over all tidal cycles considered). Instead of using an exhaustive approach [29], we applied the L-BFGS-B algorithm for Eq. (10) for τ subject to $\tau_l \leqslant \tau \leqslant \tau_u$ for each lagoon and a simulation time t_s spanning an entire year of operation. For the Swansea lagoon 16 turbines are assumed, while in the case of the Cardiff Lagoon an additional variable to be determined is the number of 30 MW turbines ($60 \leqslant N \leqslant 100$), considering that the installed capacity has been suggested to be in the range of $1.8 – 3.0$ GW. Simulations consider two operation strategies: Two-Way generation (TW) and Two-Way generation with Pumping (TWP). The 0-D models were forced using tidal elevation signals reconstructed from eight tide constituents drawn from the Bristol Channel model (Table 5) over an annual period commencing from 6/5/2003 onwards. The outputs of this optimisation deliver uniform control parameters over the entire annual period and are presented in Table 6.

As a second stage to converge towards improved control of the power plants in time, the uniform values from Table 6 are now used as an initial guess for τ_i (where i indexes every tidal cycle) in the operational control optimisation performed for every tidal cycle as per Eq. (11). Each τ_i is in turn optimised using the 0-D model commencing from the final H and m from the previous cycle. In this manner, the strategy acknowledges the history of the operation, while L-BFGS-B aims to operate the plant efficiently based on the current cycle's operation goal; in this case maximising the energy output.

The 0-D predictions according to the tide constituents of Table 5 suggest significant opportunities through an adaptive operation. The uniform operation parameters in TW_0 (Table 6) correspond to an annual energy output for the Swansea Bay and Cardiff Lagoons of 0.43 and 3.92 TW h respectively. The addition of pumping (TWP_0) results in superior energy yields: 0.55 and 4.45 TW h; a respective $\approx 28\%$ and 13.5% improvement compared to TW_0. Further to this, the optimised control of each individual cycle results in yields of 0.58 and 5.01 TW h
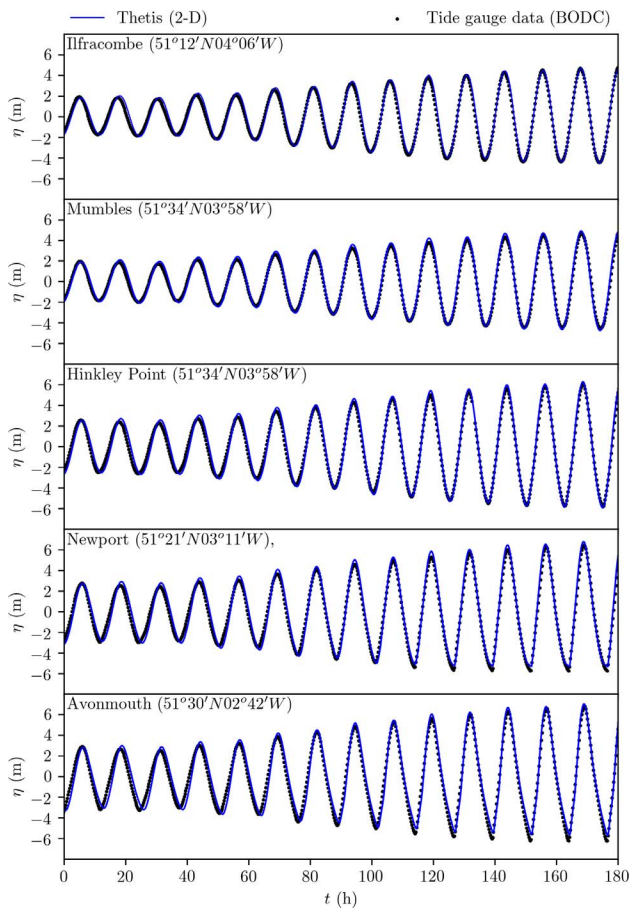
Fig. 3. Comparison of 2-D model predictions against tide gauge data for established hydrodynamics in the Severn Estuary and the Bristol Channel.

respectively. In comparison to the original TW_0 operation, the new strategy suggests energy gains in the order of 35% and 28% through a more flexible control of the turbines and sluice gates.

3.3. Adaptive operation control in 2-D coastal models

The outcome of the 0-D optimisation can be used in 2-D simulations to gauge whether an adaptive operation for each cycle would benefit the overall performance of the power plants, while taking into

consideration coupling and feedback with the hydrodynamics. Initially, we consider a uniform operation based on the parameters of Table 6 to simulate scenarios TW_0 and TWP_0 over the same three month interval considered previously for the Bristol Channel model in 2-D. A harmonic analysis of the updated tide constituents demonstrates non-trivial deviations from the original Bristol Channel model (BCM) as summarised in Table 7. The differences are attributed to the impact of the schemes on the tidal dynamics and mainly the interaction of the Cardiff Lagoon with the tidal resonance within the Severn Estuary (Fig. 2). We observe that not only the presence of the structure, but to a lesser extent even the operation control has an influence on tidal dynamics as seen by the deviation among the 2-D TW_0 and 2-D TWP_0 values. This can be observed by the differences in the constituent changes predicted for TW_0 and TWP_0 which are relatively small (as it can be seen from Table 7).

The changes in tidal amplitude and phase can be fed back into the 0-D optimisation. As described above, TW_0 and TWP_0 correspond to the outputs from the optimisation using tidal signals from the ambient Bristol Channel model and assuming uniform parameters in time. TW_1 and TWP_1 are used to signify the outputs from the optimisation where control parameters are allowed to vary with each tidal cycle, but still using the tidal signal from the ambient Bristol Channel model. TW_2 and TWP_2 signify the outputs from the adaptive optimisation which makes use of the outputs from the Bristol Channel model including lagoons operating under the TW_1 and TWP_1 parameters. This process could be repeated, although only one iteration is considered here.

3.4. Tidal range energy assessment of adaptive control strategies

Consistent with the power predictions from the 0-D model runs, the control optimisation produces interesting trends within the hydrodynamics simulations and demonstrates that a uniform regulation of the hydraulic structures is not necessarily ideal. We can observe the water elevations either side of the hydraulic structure sections in Fig. 5(a,c) for the two lagoons over a neap to spring tide transition. TW_0 and TWP_0 impose the same m periods for the operation irrespective of the tidal range. TW_1, TW_2, TWP_1 and TWP_2 alter the mode duration subject to the tidal range in the current cycle as well as the operation of previous cycles to maximise power. As a result of differences in these control scenarios, generation does not occur at the same times as in TW_0/TWP_0 with the optimisation taking advantage of the partial flexibility to delay or hasten generation (e.g. the offsets in the timings of the peak power production observed in Fig. 5b,d) to meet the optimum of the objective function.

The tidal range is perceived as a primary factor that dictates the energy levels harnessed as illustrated by the potential energy

Table 4
Comparison between observed and modelled data for amplitude α (m) and phase ϕ (deg) at tide gauge stations along the Bristol Channel for the principal lunar (M_2) and solar (S_2) semidiurnal constituents, the larger lunar elliptic semidiurnal (N_2) constituent and the principal overtide constituent M_4.

Location	M_2 α(m)		S_2 α(m)		N_2 α(m)		M_4 α(m)	
	Data	Model	Data	Model	Data	Model	Data	Model
Mumbles	3.116	3.18	1.106	1.12	0.584	0.60	0.070	0.06
Ilfracombe	3.043	3.00	1.112	1.05	0.577	0.57	0.109	0.09
Hinkley-Point	3.909	4.03	1.397	1.38	0.715	0.71	0.099	0.09
Newport	4.134	4.24	1.469	1.40	0.738	0.74	0.167	0.20
Avonmouth	4.262	4.22	1.497	1.45	0.757	0.69	0.271	0.32

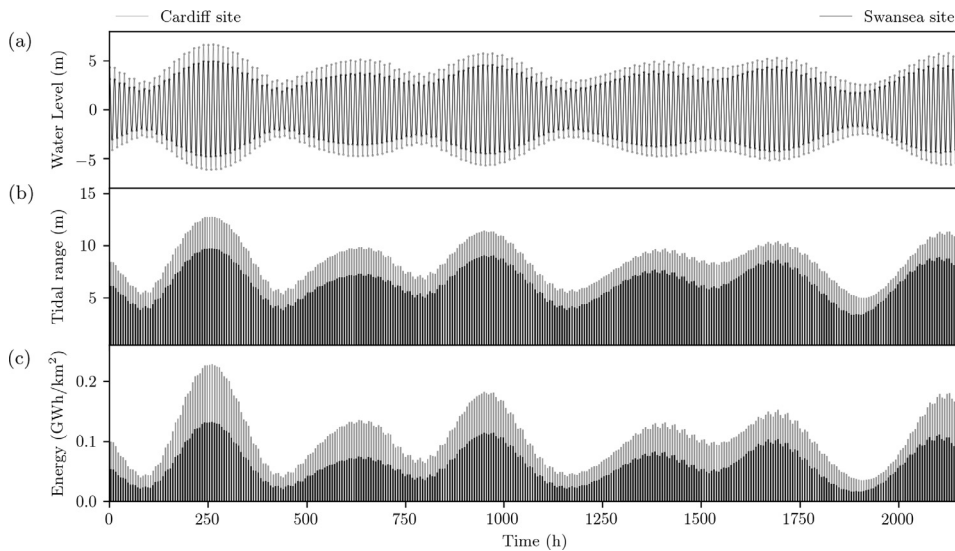| Location	M_2 ϕ(°)		S_2 ϕ(°)		N_2 ϕ(°)		M_4 ϕ(°)	
	Data	Model	Data	Model	Data	Model	Data	Model
Mumbles	172.5°	169.6°	220.3°	217.9°	154.4°	150.7°	13.9°	8.1°
Ilfracombe	161.9°	166.2°	208.7°	214.0°	143.7°	147.4°	350.9°	345.1°
Hinkley-Point	182.6°	183.3°	236.8°	236.4°	167.5°	166.2°	19.9°	12.1°
Newport	195.0°	194.5°	252.7°	251.0°	181.3°	182.1°	354.7°	324.1°
Avonmouth	201.6°	203.9°	261.6°	261.9°	188.0°	192.5°	348.9°	341.9°

Fig. 4. Variability of tidal range and corresponding potential energy contained at two prospective lagoon sites.

Table 5

Amplitude α (m) and phase ϕ (deg) at proposed locations of turbine caissons predicted during the simulations before the introduction of the tidal power plants. Note that only the four largest constituents are shown here.

Tidal Constituents	Bristol Channel model			
	Swansea Lagoon		Cardiff Lagoon	
	α(m)	ϕ(°)	α(m)	ϕ(°)
M2	3.20	169.1°	4.17	187.7°
S2	1.14	198.0°	1.47	242.3°
N2	0.61	149.5°	0.75	171.3°
K1	0.08	109.7°	0.09	117.4°

Table 6

Operation parameters obtained from the 0-D model with the optimisation of controls assumed to be uniform over a year long simulation spanning 6/5/2003 – 6/5/2004.

	Swansea Lagoon (SB)		Cardiff Lagoon (CF)		
	TW_0	TWP_0	TW_0	TWP_0	Description
N	16		71		Turbine Number
A_S	800		2400		Sluice Gate area (m^2)
t_1	0.00	0.82	0.00	0.57	Pumping duration (flood) (h)
t_2	2.82	1.76	2.87	1.67	Holding duration (flood) (h)
t_3	2.50	2.50	2.50	2.50	Generating-only duration (flood) (h)
t_5	0.00	0.93	0.00	0.80	Pumping duration (ebb) (h)
t_6	3.30	1.79	2.88	1.75	Holding duration (ebb) (h)
t_7	2.50	2.50	2.50	2.50	Generating-only duration (ebb) (h)

Table 7

Constituent amplitude α (m) and phase ϕ (deg) at proposed locations of turbine caissons predicted during the simulations following the introduction of the tidal power plants and for two different operation strategies: (a) Two-Way operation (TW_0) and (b) Two-Way operation with pumping (TWP_0). The deviations from the established tide constituents of Table 5 are included in brackets (the values in italics) to illustrate the effect of the plant operation on tidal constituent amplitudes and phases. Only constituents with noticeable changes post-construction are reported for brevity.

	Swansea Lagoon		Cardiff Lagoon	
	α(m); ($\delta\alpha$)	ϕ(°); ($\delta\phi$)	α(m); ($\delta\alpha$)	ϕ(°); ($\delta\phi$)
(a)		Two-way operation (TW)		
M2	3.15 *(−0.05)*	169.1 *(0.04)*	3.93 *(−0.24)*	185.7 *(−1.98)*
S2	1.12 *(−0.02)*	197.4 *(−0.52)*	1.36 *(−0.11)*	237.4 *(−4.97)*
N2	0.60 *(−0.01)*	149.1 *(−0.47)*	0.71 *(−0.04)*	166.5 *(−4.84)*
K1	0.08 *(−0.00)*	109.9 *(0.16)*	0.09 *(−0.00)*	117.4 *(−0.01)*
(b)		Two-way operation & pumping (TWP)		
M2	3.14 *(−0.05)*	169.2 *(0.15)*	3.90 *(−0.27)*	185.9 *(−1.80)*
S2	1.12 *(−0.02)*	197.2 *(−0.76)*	1.35 *(−0.12)*	236.5 *(−5.83)*
N2	0.60 *(−0.01)*	149.0 *(−0.56)*	0.72 *(−0.04)*	165.8 *(−5.52)*
K1	0.08 *(−0.00)*	109.9 *(0.24)*	0.09 *(−0.00)*	117.7 *(0.30)*

strategy is preferable at extreme low tides with bi-directional pumping becoming efficient as the tidal range gradually grows towards spring tides.

A comparison of the energy gains/losses for the adaptive control relative to the uniformly optimised operation (TW_0 and TWP_0) is presented in Fig. 7. In the top row we can see the predictions from the 0-D and 2-D models for the energy produced in each cycle. This provides an appreciation of the variability of the tide, but also demonstrates that for the vast majority of the cycles pumping is consistently able to deliver more energy than conventional two-way operation without pumping. In the second row we normalise the energy from TW_0 and TWP_0 with each cycle's theoretical potential energy Eq. (1) and it appears that typically 30–50% of this crude estimate can be harnessed on average, with the power plant being more inefficient during low neap tides. The averaged values of these distributions suggests that two-way operation harnesses 35% and 40% of the potential energy for Swansea and Cardiff respectively. The inclusion of pumping increases these to $\approx 46\%$ in both cases.

The bottom two rows of Fig. 7 examine how the adaptive optimisation affects the energy output in each cycle. For the optimised two-way operation outputs, the energy is compared relative to the TW_0 case. The optimisation leads to energy gains when assessed with respect to 2-D simulations, although there are differences between the 0-D and 2-D
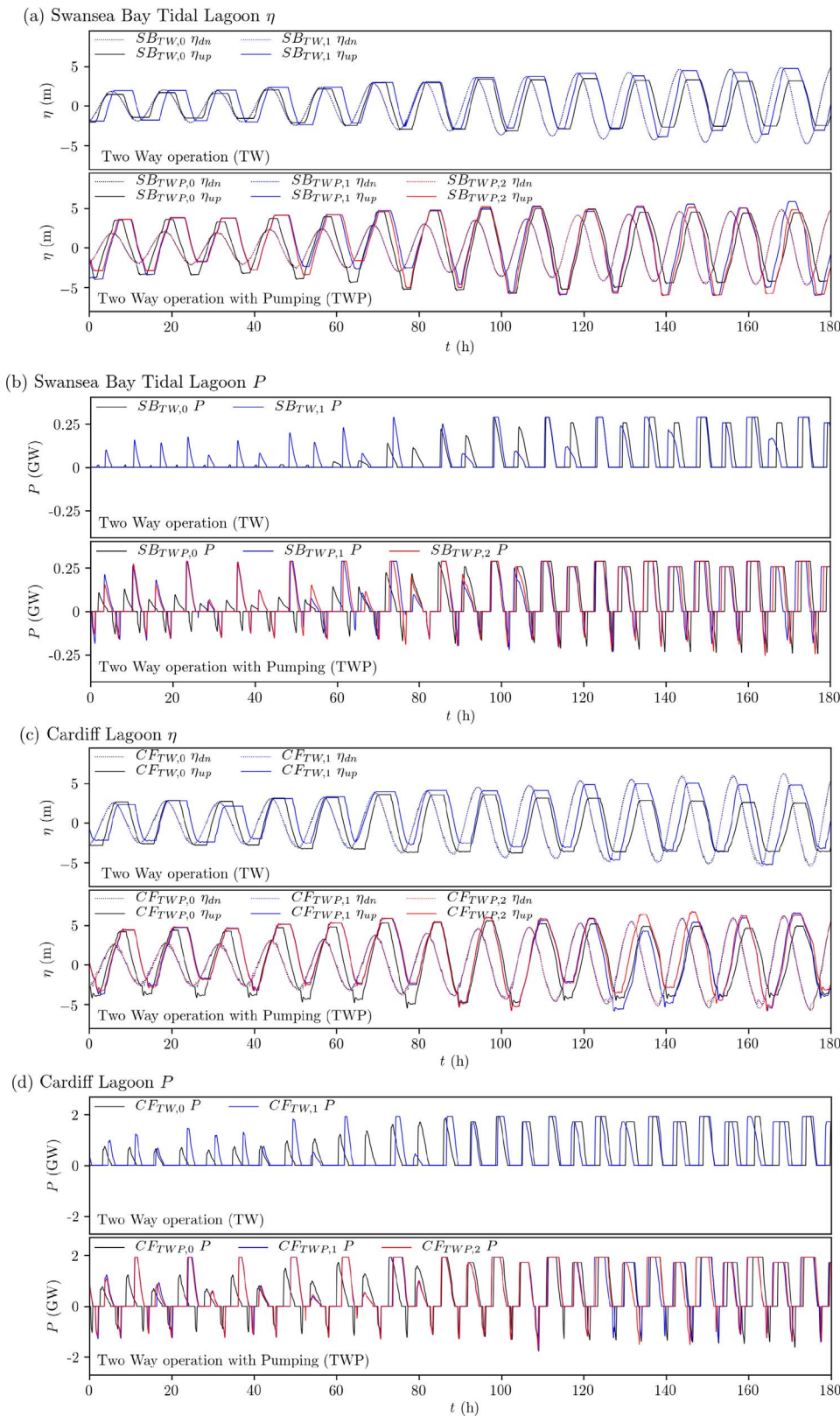
calculation through Eq. (1). In Fig. 6 we plot holding and pumping mode durations recorded for each cycle from optimised simulations (TW_2 and TWP_2) against the mean tidal range to identify patterns in control parameters during neap and spring tide conditions. The optimisation prioritises generation at ebb tide (Fig. 5b,d). This is also suggested in Fig. 6 by the greater ebb holding period, and in the case of pumping with more energy invested in order to generate during ebb tides. There are several reasons for this; for example, the turbine parametrisation assumes a 10% penalty on flood generation efficiency associated with the orientation of the turbines. In particular, at neap tides flood generation is sometimes skipped altogether (as is seen by the zero value timings in the plots) and flood pumping is the first mode to be typically omitted from the cycle. Interestingly, an ebb-pumping

(a) Swansea Bay Tidal Lagoon η

(b) Swansea Bay Tidal Lagoon P

(c) Cardiff Lagoon η

(d) Cardiff Lagoon P

Fig. 5. Predictions from the 2-D *Thetis* simulations of water elevations upstream/ downstream and power predicted for the different operation strategies of the Swansea Bay and Cardiff Lagoons. For two-way operation, TW_2 results are omitted for clarity as they effectively coincide with TW_1.

estimates of these gains. For 0-D Swansea and Cardiff predictions 57% and 54% of the potential energy is extracted respectively, whereas 2-D predictions yield energy gains of 56% and 50%. Even though the optimisation delivers notable improvement to the overall performance of the plant at neap and spring tides, there are some marginal losses during intermediate tides. The losses relative to a uniform operation are

attributed to the effect of the optimised preceding cycles on the starting conditions of subsequent ones, which can compromise the capability of the plant to harness more of the cycle's available energy.

Table 8 summarises the cumulative energy estimates from 2-D simulations with different operation scenarios. For two-way operation, the optimisation leads to $\approx 9.7\%$ and $\approx 4.2\%$ improvements for the
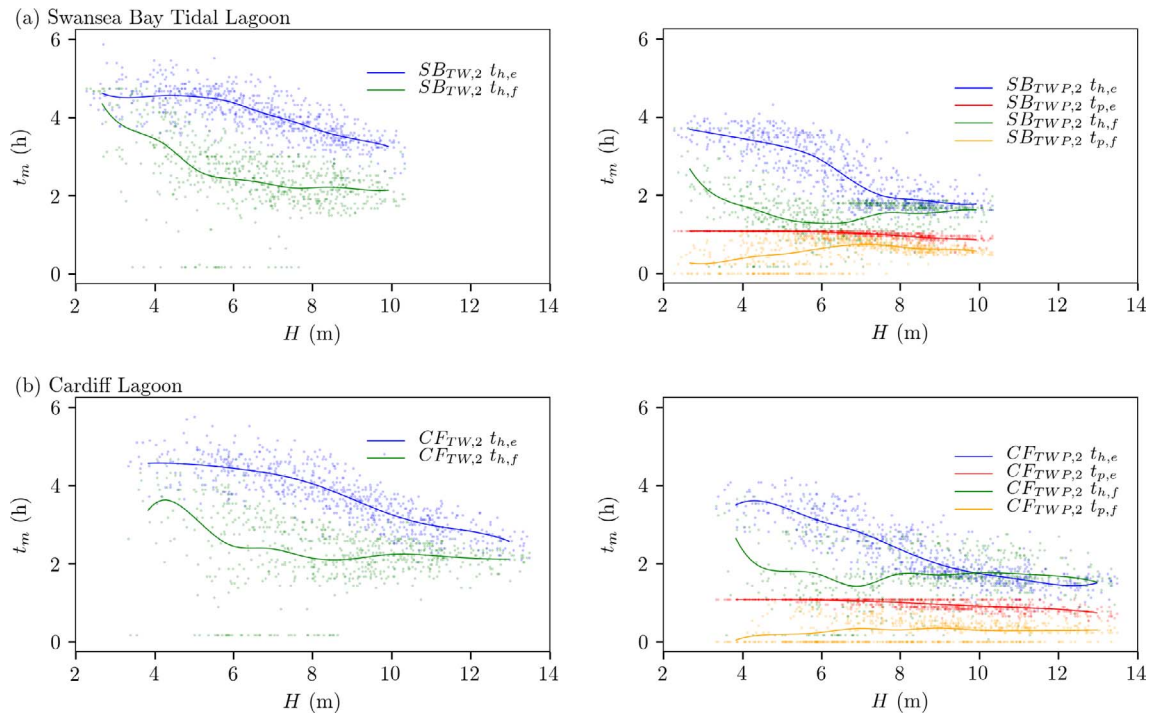
Fig. 6. Holding and pumping duration for each tidal cycle following the second round of optimisation. $t_{h,e}$ = holding duration in ebbing tide (t_6), $t_{h,f}$ = holding duration in flooding tide (t_2), $t_{p,e}$ = pumping duration at ebbing tide (t_5) and $t_{p,f}$ = pumping duration at flood tide (t_1).

Swansea Bay and Cardiff lagoons respectively. In the case of pumping, the improvement is ≈ 10.5% and ≈ 5.8%. In both operation strategies the optimisation has a greater influence on the smaller lagoon, though considering the investment associated with these projects any improvement can have a meaningful impact on the feasibility of the schemes. The consideration of both pumping and adaptive operation in time (i.e. comparing TWP_2 with TW_0) results in enhanced efficiencies of 39.8% and 23.0% for the Swansea Bay and Cardiff Lagoons respectively compared to the conventional two-way operation. The optimisation using the 0-D model yields noticeable energy gains when estimated using the 2-D simulations, providing confidence in the validity of these results. As expected, the agreement is slightly worse for the larger lagoon which is consistent with observations [27] suggesting that for large schemes 0-D results over-predict energy outputs compared to 2-D models. This indicates that while 0-D optimisation is very valuable, future work should seek to fully couple it with respect to 2-D (and potentially even 3-D) hydrodynamics.

3.5. Methodology capabilities & applications

A method to assess and optimise future tidal power plant installations has been developed which exploits adaptive plant operation. Compared to earlier approaches (e.g. [6,14]) we present extensions that consider a set of tunable parameters that arise during each tidal cycle, thus rendering a more flexible operation scheduling; this enables switching between ebb-only, flood-only and two-way strategies with or without pumping, while taking into consideration the capabilities of the installed turbines and sluice gates. These refinements reflect the potential of new turbine technologies to yield superior pumping efficiencies [26]. Taking into account the tidal range variability in time (Fig. 4), it has been demonstrated how adaptive operation strategies can deliver superior energy outputs (Table 8) that can make a difference in the competitiveness of marine energy proposals. This would be in the form of facilitating energy gains with no additional investment, thus lowering the potentially high subsidies associated with pilot and small-scale schemes.

The energy maximisation optimisation framework can be readily

extended to consider further important factors such as matching energy demand or environmental impact mitigation strategies over the lifetime of prospective tidal energy designs by altering the objective function in Eq. (11). Developers and engineers can also replace the study's turbine parametrisation with specifications of their proposed technology to optimise their design's operation. In turn, given the necessary input to force the hydrodynamics models and predict the necessary water level time series, the 0-D model can easily converge to the main design parameters (as in Section 3.2) and inform 2-D simulations that also account for hydrodynamic impacts. Feeding the resultant scheduling parameters to coastal models demonstrates the importance of fully coupling optimisation with the hydrodynamics as larger schemes are considered. In particular, hydrodynamic simulations in previous studies only spanned from a few tidal cycles [41,24,42] to as long as a single lunar month [27], rather than testing the designs over extended periods as in the three lunar month period considered here. Scaling the 2-D energy output according to year-long 0-D simulations as in Table 8 produces annual predictions that account for the variability of the tides over the entire annual period. In this manner, the methodology described can be re-applied to optimise other prospective tidal power plant designs.

4. Conclusions

This paper has presented a methodology for the optimisation of tidal range power plant operation. Initially, we acknowledge the variability of the tides and demonstrate how a plant's operation can be controlled to deliver partial flexibility in the timing of its power generation. This paves the way towards an optimisation problem where control parameters need to be determined over time to meet the objectives of the operation. We propose a methodology employing gradient-based optimisation coupled with a generalised 0-D power plant operation model to determine operation parameters yielding improved performance for each tidal cycle. Subsequently, the control parameter values for each cycle can be used within more computationally intensive hydrodynamic models that have the capability to simulate the operation of tidal lagoons and barrages while also accounting for the hydrodynamic
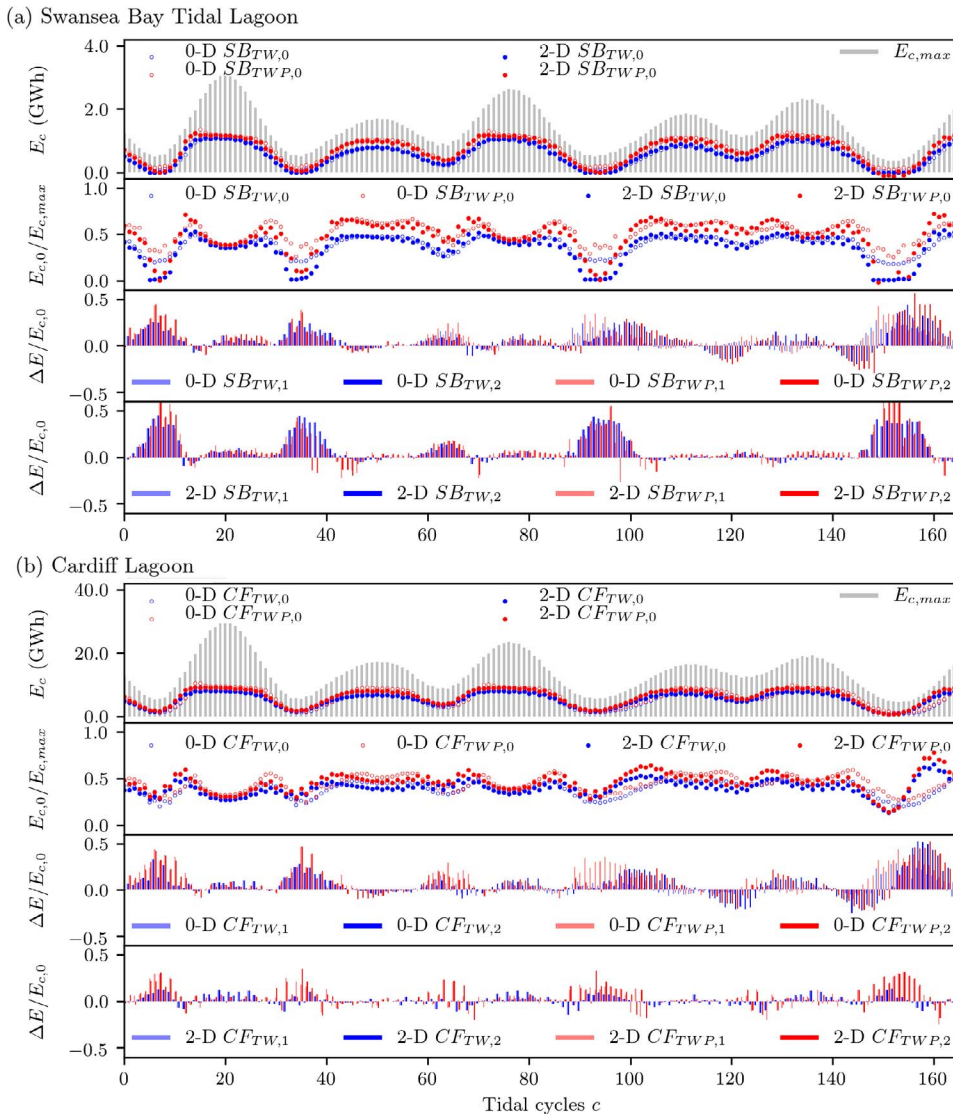
Fig. 7. Overview of energy output from (a) the Swansea Bay Tidal Lagoon and (b) the Cardiff Lagoon. Top two rows: Energy extracted per cycle (E_c) plotted with each cycle's theoretical available energy ($E_{c,max}$), as well as the ratios of these quantities, for the TW_0 and TWP_0 cases. Bottom two rows: benefits of adaptive operation as predicted by the 0-D and 2-D models where $\Delta E = E_{c,i} - E_{c,0}$ where $i \in \{1,2\}$ is the index of the adaptive optimisation iteration.

Table 8

Energy output from 2-D *Thetis* simulations for the two lagoon case studies. E_{2D} = energy accumulated during the three month simulation period. $\frac{E_{2D} - E_{0D}}{E_{0D}}$ = percentile deviation of 2-D model results from 0-D estimates. E_{yr} = projected annual energy from the 2-D results obtained by using the deviation between 2-D and 0-D values over the 3 month period to scale the computed annual energy output obtained from the 0-D model.

	Swansea Bay Tidal Lagoon				Cardiff Lagoon			
	E_{2D} (TW h)	$\frac{E_{2D} - E_{0D}}{E_{0D}}$ %	E_{yr} (proj.) (TW h)	$\frac{E_{2D}}{E_{max}}$ %	E_{2D} (TW h)	$\frac{E_{2D} - E_{0D}}{E_{0D}}$ %	E_{yr} (proj.) (TW h)	$\frac{E_{2D}}{E_{max}}$ %
TW_0	0.101	−2.70	0.417	39.73	0.952	−2.04	3.829	39.21
TW_1	0.111	0.06	0.463	43.58	0.992	−3.87	4.164	40.89
TW_2	0.111	−2.59	0.440	43.57	0.992	−8.07	3.940	40.89
TWP_0	0.127	−5.13	0.515	50.23	1.106	0.35	4.442	45.59
TWP_1	0.141	−2.80	0.569	55.47	1.165	−5.49	4.734	48.01
TWP_2	0.141	−3.43	0.555	55.53	1.171	−4.65	4.734	48.24

response to the structure.

The study considers the simultaneous operation of two prospective tidal lagoons for the Bristol Channel and the Severn Estuary, UK. These are the Swansea Bay and the Cardiff Tidal Lagoons proposed by Tidal Lagoon Power Ltd. The optimisation results correspond to noticeable improvements in the tidal plants' performance, even though it is clear that fully coupling the hydrodynamics within the optimisation could deliver further benefits. This was demonstrated by consecutively applying the optimisation strategy on tidal signals that were altered by the presence of the lagoons. Overall, scenarios where operation is optimised per cycle and pumping included lead to a 20–40% improvement in comparison with a conventional two-way uniform operation for the considered case studies.

Looking ahead and with more projects proposed in the near future, there is an incentive to refine the methodology presented here to be efficiently linked with hydrodynamic models and thus thoroughly acknowledge the hydrodynamic response caused by the presence of marine infrastructure. Moreover, the objective function considered here

was simple but in due course can be extended to acknowledge transient demand and/or environmental impacts in order to maximise the societal benefit of the schemes while ensuring a sustainable integration of marine energy infrastructure in coastal waters. Finally, subsequent work should focus on efficiently optimising the operation in a manner that acknowledges the potential implications of current control parameters on the plant performance during subsequent tidal cycles.

Acknowledgements

References

[1] Xia J, Falconer RA, Lin B. Impact of different operating modes for a Severn Barrage on the tidal power and flood inundation in the Severn Estuary, UK. Appl Energy 2010;87:2374–91.
[2] Hooper T, Austen M. Tidal barrages in the UK: ecological and social impacts, potential mitigation, and tools to support barrage planning. Renew Sustain Energy Rev 2013;23:289–98.
[3] Waters S, Aggidis G. Tidal range technologies and state of the art in review. Renew Sustain Energy Rev 2016;59:514–29.
[4] Hendry C. The role of tidal lagoons, Technical Report, UK Government; 2017. <https://hendryreview.com/>.
[5] Wolf J, Walkington IA, Holt J, Burrows R. Environmental impacts of tidal power schemes. Proc ICE Maritime Eng 2009;162:165–77.
[6] Aggidis G, Benzon D. Operational optimisation of a tidal barrage across the Mersey estuary using 0-D modelling. Ocean Eng 2013;66:69–81.
[7] O Rourke F, Boyle F, Reynolds A. Tidal energy update 2009. Appl Energy 2010;87:398–409.
[8] Prandle D. Simple theory for designing tidal power schemes. Adv Water Resources 1984;7:21–7.
[9] Burrows R, Walkington I, Yates N, Hedges T, Wolf J, Holt J. The tidal range energy potential of the West Coast of the United Kingdom. Appl Ocean Res 2009;31:229–38.
[10] Xia J, Falconer RA, Lin B. Hydrodynamic impact of a tidal barrage in the Severn Estuary, UK. Renewable Energy 2010;35:1455–68.
[11] Xia J, Falconer Ra, Lin B. Impact of different tidal renewable energy projects on the hydrodynamic processes in the Severn Estuary, UK. Ocean Model 2010;32:86–104.
[12] Falconer RA, Xia J, Lin B, Ahmadian R. The Severn Barrage and other tidal energy options: hydrodynamic and power output modeling. Sci China Ser E: Technol Sci 2009;52:3413–24.
[13] Cornett A, Cousineau J, Nistor I. Assessment of hydrodynamic impacts from tidal power lagoons in the Bay of Fundy. Int J Mar Energy 2013;1:33–54.
[14] Lisboa A, Vieira T, Guedes L, Vieira D, Saldanha R. Optimal analytic dispatch for tidal energy generation. Renewable Energy 2017;108:371–9.
[15] Vieira D, Guedes L, Lisboa A, Saldanha R. Formulations for hydroelectric energy production with optimality conditions. Energy Convers Manage 2015;89:781–8.
[16] Angeloudis A, Piggott MD, Kramer SC, Avdis A, Coles D. Comparison of 0-D, 1-D and 2-D model capabilities for tidal range energy resource assessments. In: EWTEC 2017, Cork; 2017. p. 1–10.
[17] Culley DM, Funke SW, Kramer SC, Piggott MD. Integration of cost modelling within the micro-siting design optimisation of tidal turbine arrays. Renewable Energy 2016;85:215–27.
[18] Funke S, Farrell P, Piggott M. Tidal turbine array optimisation using the adjoint approach. Renewable Energy 2014;63:658–73.
[19] du Feu R, Funke S, Kramer S, Culley D, Hill J, Halpern B, et al. The trade-off between tidal-turbine array yield and impact on flow: a multi-objective optimisation problem. Renewable Energy 2017;114:1247–57.
[20] Angeloudis A, Falconer R, Bray S, Ahmadian R. Representation and operation of tidal energy impoundments in a coastal hydrodynamic model. Renewable Energy 2016;99:1103–15.
[21] Baker A. Tidal power. IEE Proc A Phys Sci Meas Instrum Manage Edu Rev 1987;134:392.
[22] Lee DS, Oh S-H, Yi J-H, Park W-S, Cho H-S, Kim D-G, et al. Experimental investigation on the relationship between sluice caisson shape of tidal power plant and the water discharge capability. Renewable Energy 2010;35:2243–56.
[23] Oh S-H, Lee KS, Jeong W-M. Three-dimensional experiment and numerical simulation of the discharge performance of sluice passageway for tidal power plant. Renewable Energy 2016;92:462–73.
[24] Bray S, Ahmadian R, Falconer RA. Impact of representation of hydraulic structures in modelling a severn barrage. Comput Geosci 2016;89:96–106.
[25] Aggidis G, Feather O. Tidal range turbines and generation on the solway firth. Renewable Energy 2012;43:9–17.
[26] Yates N, Walkington I, Burrows R, Wolf J. The energy gains realisable through pumping for tidal range energy schemes. Renewable Energy 2013;58:79–84.
[27] Angeloudis A, Falconer RA. Sensitivity of tidal lagoon and barrage hydrodynamic impacts and energy outputs to operational characteristics. Renewable Energy 2017;114(A):337–51.
[28] Lewis M, Angeloudis A, Robins P, Evans P, Neill S. Influence of storm surge on tidal range energy. Energy 2017;122:25–36.
[29] Angeloudis A, Ahmadian R, Falconer RA, Bockelmann-Evans B. Numerical model simulations for optimisation of tidal lagoon schemes. Appl Energy 2016;165:522–36.
[30] Rathgeber F, Ham DA, Mitchell L, Lange M, Luporini F, Mcrae ATT, et al. Firedrake: Automating the finite element method by composing abstractions. ACM Trans Math Softw 2016;43:24:1–24:27.
[31] Kärnä T, de Brye B, Gourgue O, Lambrechts J, Comblen R, Legat V, et al. A fully implicit wetting-drying method for DG-FEM shallow water models, with an application to the Scheldt Estuary. Comput Methods Appl Mech Eng 2011;200:509–24.
[32] Balay S, Abhyankar S, Adams MF, Brown J, Brune P, Buschelman K, et al., PETSc Users Manual, Technical Report ANL-95/11 - Revision 3.7, Argonne National Laboratory; 2016. <http://www.mcs.anl.gov/petsc>.
[33] Zhu C, Byrd RH, Lu P, Nocedal J. Algorithm 778: L-bfgs-b: Fortran subroutines for large-scale bound-constrained optimization. ACM Trans Math Softw 1997;23:550–60.
[34] Tidal Lagoon Power turbine technology; 2017. <http://www.tidallagoonpower.com/tidal-technology/turbine-technology/> [accessed: 15-10-2017].
[35] Tidal Lagoon Power Development Consent Application; 2017. <http://www.tidallagoonpower.com/application-for-development-consent/> [accessed: 15-10-2017].
[36] Tidal Lagoon Power Cardiff Lagoon; 2017. <http://www.tidallagoonpower.com/projects/cardiff/planning/> [accessed: 15-10-2017].
[37] Avdis A, Candy AS, Hill J, Kramer SC, Piggott MD. Efficient unstructured mesh generation for marine renewable energy applications. Renewable Energy 2017.
[38] Avdis A, Jacobs CT, Mouradian SL, Hill J, Piggott DM. Meshing ocean domains for coastal engineering applications, ECCOMAS; 2016. doi:http://dx.doi.org/10.7712/100016.1830.7712.
[39] Edina Digimap Service, Hydrospatial one, gridded bathymetry. SeaZone Solutions Ltd; 2014. <http://digimap.edina.ac.uk/marine/> [Online; accessed 2017].
[40] Egbert GD, Erofeeva SY. Efficient inverse modeling of barotropic ocean tides. J Atmos Oceanic Technol 2002;19:183–204.
[41] Xia J, Falconer RA, Lin B, Tan G. Estimation of annual energy output from a tidal barrage using two different methods. Appl Energy 2012;93:327–36.
[42] Zhou J, Pan S, Falconer Ra. Optimization modelling of the impacts of a Severn Barrage for a two-way generation scheme using a Continental Shelf model. Renewable Energy 2014;72:415–27.